

# **Analysis of the October 2005 proton test data on the low-stress module**

**Martin Groenewegen (ICC KUL)**

DOCUMENT CHANGE RECORD

Version	Date	Changes	Remarks
Draft 0	01-January-2006	–	start of document
Draft 1	03-April-2006	all	released to PACS-ICC

## Reference Documents

RD 1 – Test Plan and procedure for investigation of glitch event rate and collected charge variation in the Ge:Ga detectors during proton irradiation at UCL-CRC (3rd test phase, PACS-ME-TP-009, issue 3.1, 2 October 2005, Katterloher, Barl & Royer

RD 2 – Analysis of the April 2005 proton test data, PICC-KL-TN-020, draft 1, Dec. 2005 Groenewegen & Royer (KUL),

RD 3 – Fitting PACS ramps with analytical models. Part III: The IMEC model, PICC-KL-TN-010, draft 2, May 2005, M.A.T. Groenewegen

RD 4 – Testing Glitch Detection Algorithms by Monte-Carlo Simulations, PICC-KL-TN-019, draft 1, Oct. 2005, Groenewegen et al.

RD 5 – UCL-CRC Proton tests of March 2004: glitch height distribution, PICC-KL-TN-012, draft 2, march 2005, M.A.T. Groenewegen

RD 6 – FM proton irradiation tests high & low stress modules I: Glitch effects & curing, PICC-KL-TN-022, draft 1, Jan. 2006, P. Royer

RD 7 – Geant 4 simulations of GeGa module behaviour under proton irradiation. Part II Tests of April 2005, PICC-TS-SIM-005, Issue 1, Jan. 2006, Bongardo & Andreani

## 1. Introduction

This report focuses on the third phase of the proton irradiation tests which took place in the cyclotron at Louvain-La-Neuve (UCL-CRC) between 3 and 5 October 2005, and which is described in RD 1.

Discussed are however not only issues related to glitches and the effect of radiations but also on the pre-irradiation data as this is the first time there is data available on the latest generation of CREs for the low-stress detectors.

## 2. Integration versus post-integration noise

The files listed in Table 1 were investigated, which are the pre-irradiation data of Oct. 4 and 5. For each file only detectors 3 and 12 were looked at, as being representative for the case with and w/o the FIR cut-on filter in front.

The mean voltage at the first read-out over the ramps is subtracted from all ramps (not doing this has no influence on the outcome). At every readout the standard deviation,  $\sigma$ , is determined over all ramps in the dataset. Figure 1 shows a representative plot of how the noise develops as a function of read-out for the highest and lowest capacitor settings.

The prediction is that the noise would go like:  $\sigma^2 = (\sigma_p)^2 + j (\sigma_i)^2$  as a function of read-out  $j$ , where  $\sigma_p$  and  $\sigma_i$  are the post-integration and integration noise, respectively. This model was fitted to the data, and the results are listed in Table 1. The post-integration noise is found to be on average 15 times larger than the integration noise. A discussion of the standard deviation of the slopes is given in the following section. Examples of the noise versus readout are shown in Figure 1.

Table 1: Post-integration and integration noise.

file name	detector	post-integration noise ( $10^{-5}$ )	integration noise ( $10^{-6}$ )
T25b200t025c14n256_#N_1.dat	3	100.3 ± 1.4	70.8 ± 5.5
	12	127.5 ± 1.5	9.8 ± 54.
T25b200t025c07n256_#N_2.dat	3	133.8 ± 4.6	172. ± 9.7
	12	153.9 ± 2.8	173. ± 6.9
T25b200t025c04n256_#N_3.dat	3	181.9 ± 2.4	189. ± 6.4
	12	211.1 ± 4.6	215. ± 12.3
T25b200t025c03n256_#N_4.dat	3	218.7 ± 4.5	361. ± 7.4
	12	207.0 ± 9.4	483. ± 11.
T25b120t025c14n256_#N_5.dat	3	102.3 ± 1.5	44.3 ± 9.8
	12	125.7 ± 1.6	40.7 ± 14.
T25b120t025c07n256_#N_6.dat	3	127.0 ± 1.6	80.7 ± 6.8
	12	150.0 ± 2.0	101. ± 8.1
T25b120t025c04n256_#N_7.dat	3	174.1 ± 1.9	121. ± 7.5
	12	180.1 ± 2.4	152. ± 7.9
T25b120t025c03n256_#N_8.dat	3	219.2 ± 2.3	175. ± 8.0
	12	220.5 ± 2.7	215. ± 7.6
T25b80t025c14n256_#N_9.dat	3	101.8 ± 1.3	16.8 ± 21.1
	12	124.4 ± 1.6	40.3 ± 13.7
T25b80t025c07n256_#N_10.dat	3	126.7 ± 1.5	41.7 ± 12.8
	12	146.5 ± 1.8	74.8 ± 9.7
T25b80t025c04n256_#N_11.dat	3	168.0 ± 1.7	107.1 ± 7.4
	12	184.6 ± 1.9	118.1 ± 8.1
T25b80t025c03n256_#N_12.dat	3	222.4 ± 1.6	84.0 ± 11.5
	12	225.0 ± 2.4	126.8 ± 11.7
T25b120t1c14n64_#N_13.dat	3	102.4 ± 1.5	27.1 ± 4.0
	12	129.8 ± 1.6	24.2 ± 5.9
T25b120t05c14n128_#N_14.dat	3	99.6 ± 1.5	36.0 ± 5.8
	12	126.7 ± 1.6	27.3 ± 10.2
T25b120t025c14n256_#N_15.dat	3	99.0 ± 1.3	40.9 ± 8.6
	12	122.5 ± 1.3	53.9 ± 7.9
T25b120t0125c14n512_#N_16.dat	3	99.1 ± 1.3	62.7 ± 11.6
	12	124.4 ± 1.6	48.0 ± 23.
T25b120t00625c14n1024_#N_17.dat	3	104.9 ± 1.2	-----
	12	121.3 ± 1.7	115.3 ± 20.2
T25b120t025c14n256_#N_27.dat	3	100.2 ± 1.4	43.7 ± 9.1
	12	124.9 ± 1.4	56.5 ± 8.6
T25b120t025c07n256_#N_28.dat	3	126.3 ± 2.2	113.3 ± 6.7
	12	146.9 ± 2.1	98.8 ± 8.4
T25b120t025c04n256_#N_29.dat	3	169.1 ± 2.2	138. ± 7.4
	12	173.8 ± 2.7	191. ± 6.7
T25b120t025c03n256_#N_30.dat	3	206.2 ± 2.8	254. ± 6.3
	12	211.5 ± 3.4	240. ± 8.3
T25b80t025c14n256_#N_31.dat	3	100.4 ± 1.5	39.2 ± 10.8
	12	126.6 ± 1.5	24.8 ± 22.2
T25b80t025c07n256_#N_32.dat	3	123.2 ± 1.4	61.5 ± 7.9
	12	145.0 ± 1.6	68.5 ± 9.3
T25b80t025c04n256_#N_33.dat	3	161.1 ± 1.4	82.1 ± 7.7
	12	177.6 ± 2.0	136.1 ± 7.2
T25b80t025c03n256_#N_34.dat	3	217.4 ± 2.4	100.1 ± 1.4
	12	220.0 ± 2.1	170.7 ± 7.6

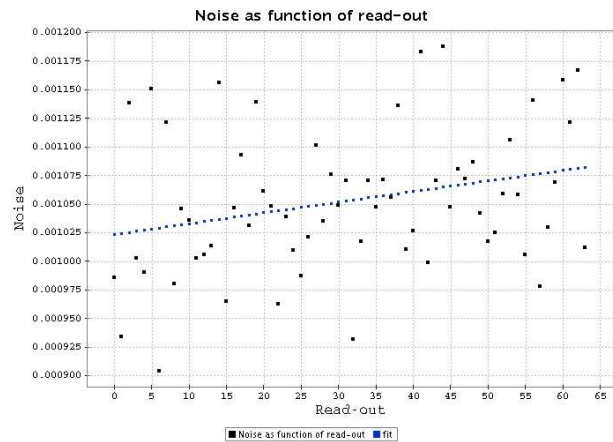
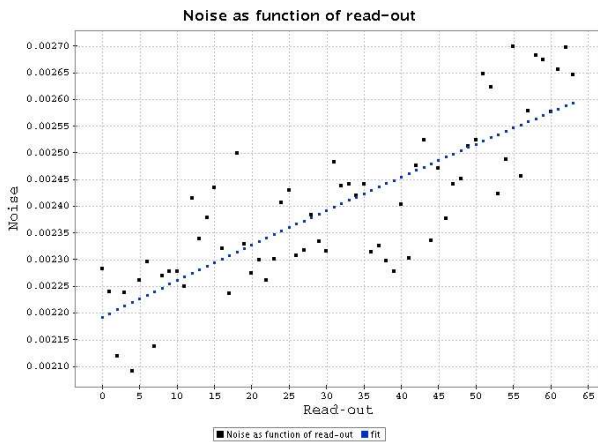


Figure 1: Noise as a function of read-out for detector 3 in files T25b120t025c03n256\_N\_8.dat (left) and T25b120t025c14n256\_N\_5.dat (right).

Table 2: Post-integration and integration noise *with detector zero subtracted*.

filename	detector	post-integration noise ( $10^{-5}$ )	integration noise ( $10^{-6}$ )
T25b120t025c14n256.#N_5.dat	3	$114.6 \pm 2.5$	$39.6 \pm 19.8$
	12	$157.4 \pm 1.8$	$34.0 \pm 23.7$
T25b120t025c07n256.#N_6.dat	3	$129.2 \pm 2.3$	$64.8 \pm 12.5$
	12	$168.0 \pm 1.9$	$95.9 \pm 8.8$
T25b120t025c04n256.#N_7.dat	3	$154.1 \pm 2.4$	$103. \pm 9.7$
	12	$179.3 \pm 2.0$	$142. \pm 7.0$
T25b120t025c03n256.#N_8.dat	3	$198.9 \pm 2.4$	$167. \pm 7.7$
	12	$211.3 \pm 2.5$	$202. \pm 7.2$
T25b80t025c14n256.#N_31.dat	3	$121.2 \pm 1.5$	$29.0 \pm 17.8$
	12	$138.0 \pm 1.7$	$28.0 \pm 24.0$
T25b80t025c07n256.#N_32.dat	3	$131.3 \pm 1.8$	$71.5 \pm 8.8$
	12	$149.8 \pm 1.8$	$69.9 \pm 10.5$
T25b80t025c04n256.#N_33.dat	3	$160.2 \pm 1.8$	$68.8 \pm 11.6$
	12	$170.4 \pm 2.1$	$126.0 \pm 7.8$
T25b80t025c03n256.#N_34.dat	3	$206.6 \pm 2.0$	$83.8 \pm 1.4$
	12	$207.0 \pm 2.4$	$162.8 \pm 8.4$

The analysis has been repeated by subtracting detector 0 for selected files. The results are listed and shown in Table 2 and Figure 2. The post-integration noise remains the same on average; there are examples where it is reduced, and examples where it is increased, sometimes by almost 30%, indicating that the noise in detector 0 is almost uncorrelated. The integration noise levels are reduced by 10-15%.

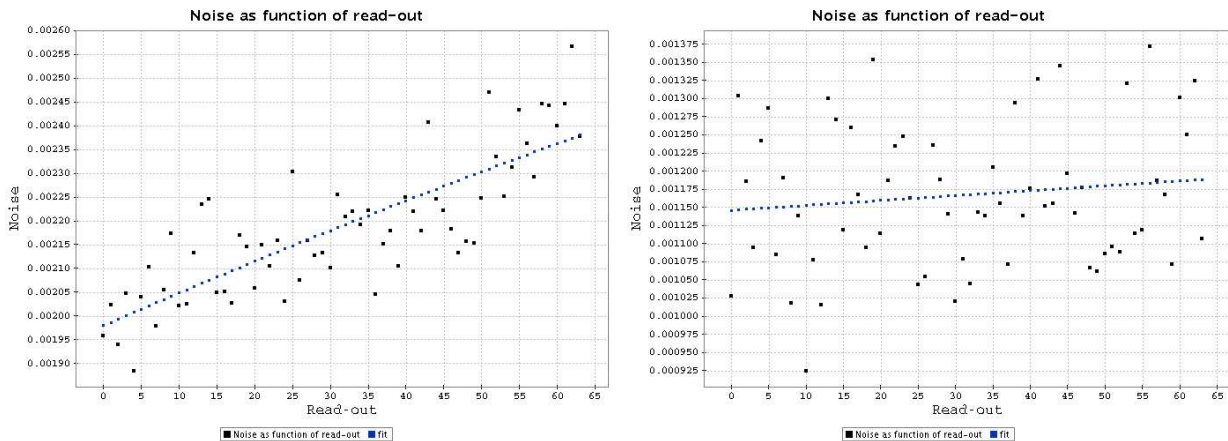


Figure 2: As figure 1 but *with detector zero subtracted*.

There are some interesting correlations which are illustrated in Figure 3 and 4. The post-integration noise depends on the capacitance value, and not on the bias value (as expected). The third plot in Figure 3 demonstrates that the post-integration noise scales like  $\frac{1}{C_f}$ , as was found in RD 2 for the high-stressed detectors.

The integration noise depends on bias, capacitance, and signal strength. Empirically it is found that the quantity (integrating noise  $\times (-slope)^{-0.7}$ ) becomes almost constant and independent of bias, capacitance, and signal strength.

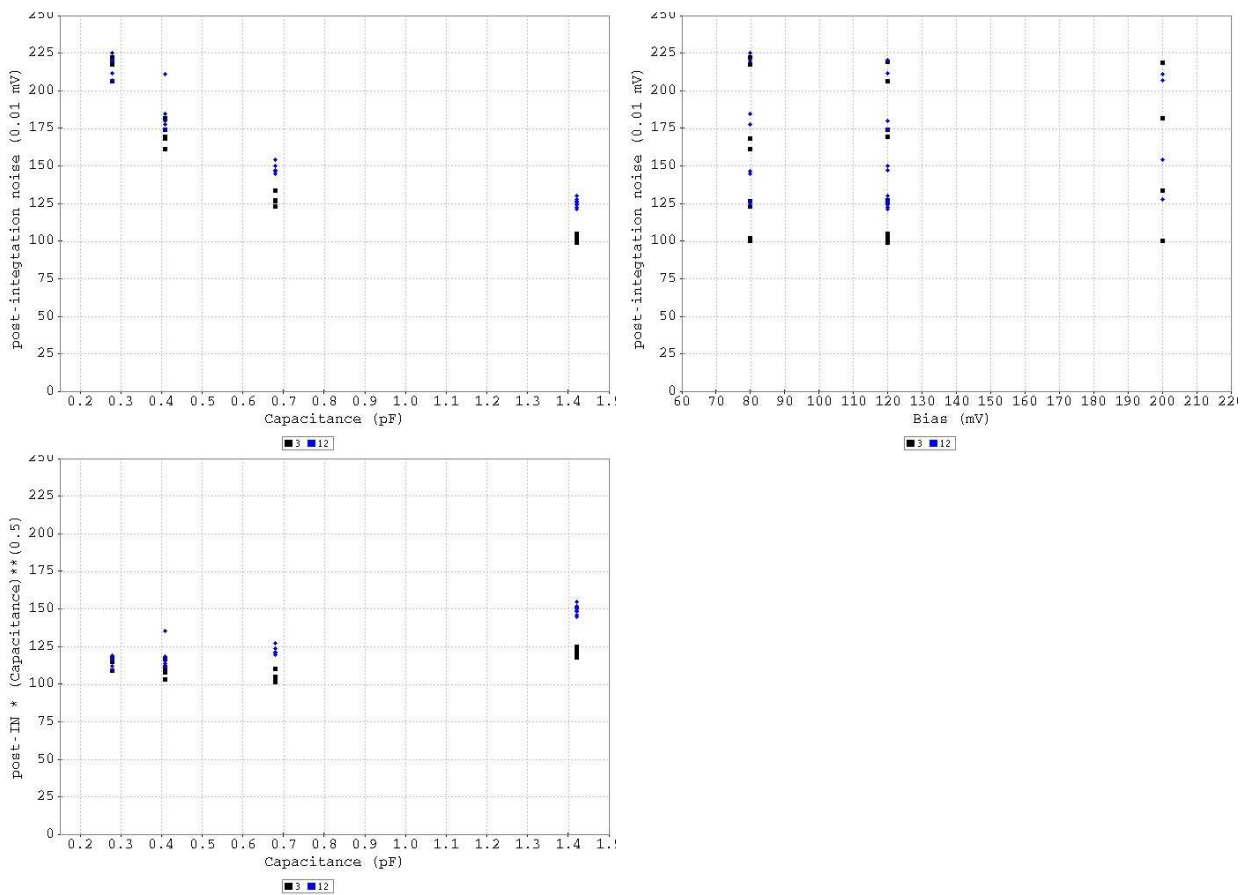


Figure 3: Post-Integrating noise (PIN) for detectors 3 (black) and 12 (red) as a function of bias and capacitor settings.

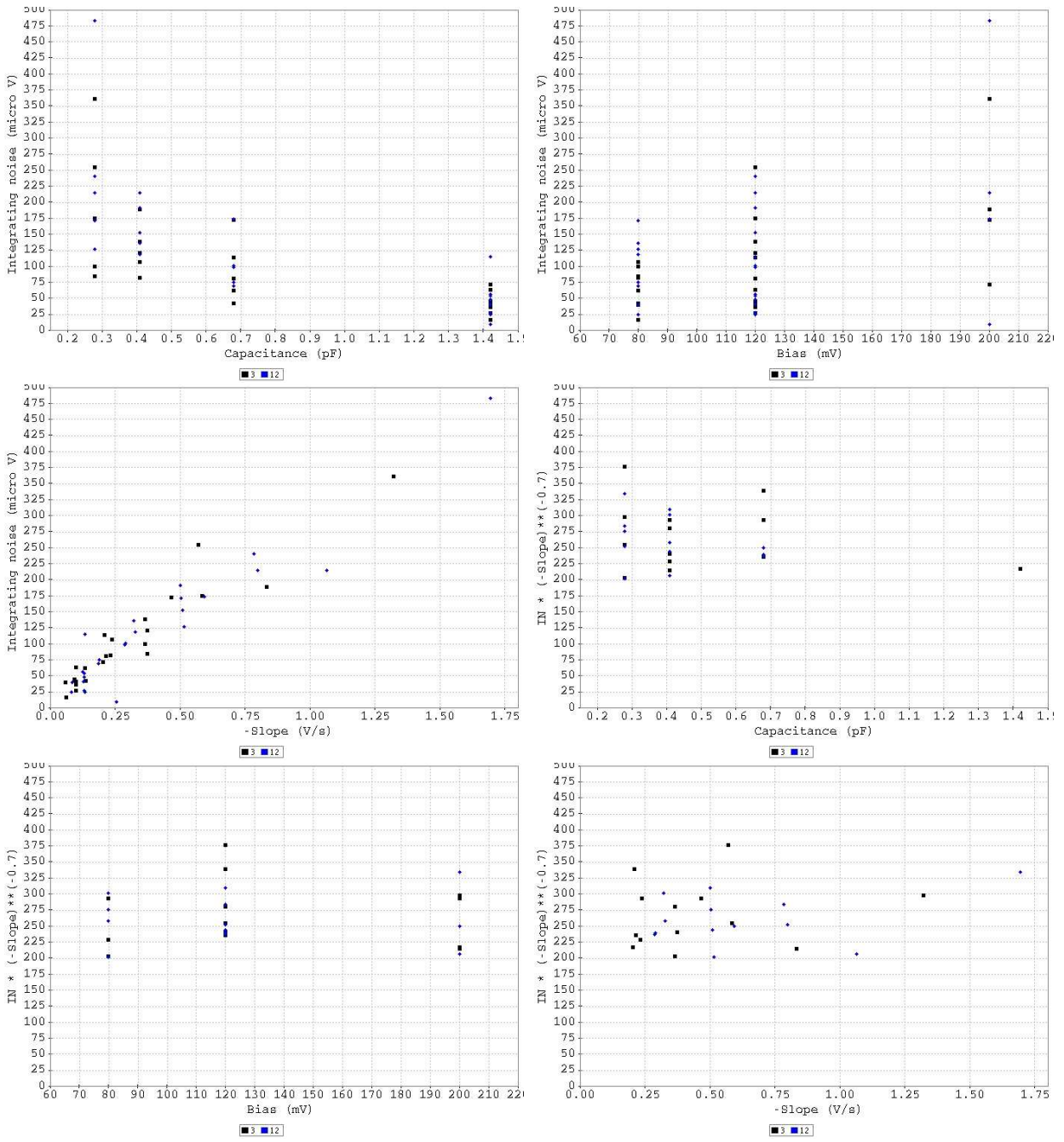


Figure 4: Integration noise for detectors 3 (black) and 12 (red) as a function of bias and capacitor settings.

### 3. Overall shape of the ramps

The ramps have been fitted with the IMEC model of the ramps, as described in RD 3. To recall, the ramps are described as:

$$V(t) = V(0) + A (-1.0 + \exp(-t \zeta \omega) \times (\cosh(t \omega d) + (\zeta + \omega \tau)/d \times \sinh(t \omega d))) \quad (1)$$

with

$$d = \sqrt{\zeta^2 - 1}$$

where  $t$  represent time, and  $\omega$  and  $\zeta$  are known via the relations

$$\omega = 1.0 / \sqrt{(C_f + C_p) R_d \tau_c} \quad (2)$$

and

$$\zeta = \omega \times \frac{1}{2} (((1.0 + A) C_f + C_p) R_d + \tau_c) \quad (3)$$

The parameters of the model (some of which are known) are therefore:

$V(0)$ , Voltage at first read-out

$A$ , amplifier gain

$C_f$ , feedback capacitance

$C_p$ , parasitic capacitance

$R_d$ , resistance of the detector, a proxy for the power of the in-falling infra-red light

$\tau_c$ , time constant of the amplifier

$\tau$ , ad-hoc parameter, related to the “bump”

$V_b$ , bias voltage

It is also useful to define a *slope* (in units of V/s), as in the limit of infinite gain Equation (1) becomes

$$slope = \frac{dV(t)}{dt} = \frac{-V_b}{C_f R_d} \quad (4)$$

In other words,  $R_d$  is fitted, and then *slope* is calculated according to Eq. 4. The advantage is that a comparison is possible with the slopes derived by fitting a straight line to the data.

The feedback capacitance and bias value are known quantities. As quoted in RD 1, the measured capacitance for QM25– and the relation to the name in the filename–is: c03 = 0.28, c04 = 0.41, c07 = 0.68, c14 = 1.42 pF.

There is a slight tendency for a “bump” in some ramps. Nevertheless it was decided to fix  $\tau$  to zero and rather, by default, to not include the first 2 non-destructive readouts in the fitting.

$A$ ,  $C_p$  and  $\tau_c$  were kept at the values derived in RD 2 as there was no obvious reason to change them. These values are  $A = 150$ ,  $C_p = 2.0$  pF,  $\tau_c = 0.6$ .

Hence, the fitting is done with 2 free-parameters,  $V(0)$  and  $R_d$  (and thus *slope*).

In Tables 3-5, there is listed the filename, and then for detectors 3 and 12 each, 5 columns with the median value of the *slope*, the standard deviation in the *slope*, the number of function calls, reduced  $\chi^2$  returned for the fitting assuming a constant weight per read-out of  $10^6$  (i.e. an “error” of 0.001 V), and the noise determined by fitting a Gaussian to the residuals between the data and the fit.

The last column list the (S/N) for both detector 3 and 12, defined as (S/N)= mean(-slope)/stdev(slope)\*  $\sqrt{n_{slopes}}$ . Some clear trends are obvious: in the pre-irradiation data the best (S/N) are achieved for (1) the highest bias tested, namely 200 mV, (2) for a given bias, a capacitance of 0.3 or 0.4 pF, and (3) for the longest ramp-length of 1 second.

Figure 5 shows some examples of ramps, and the fits.

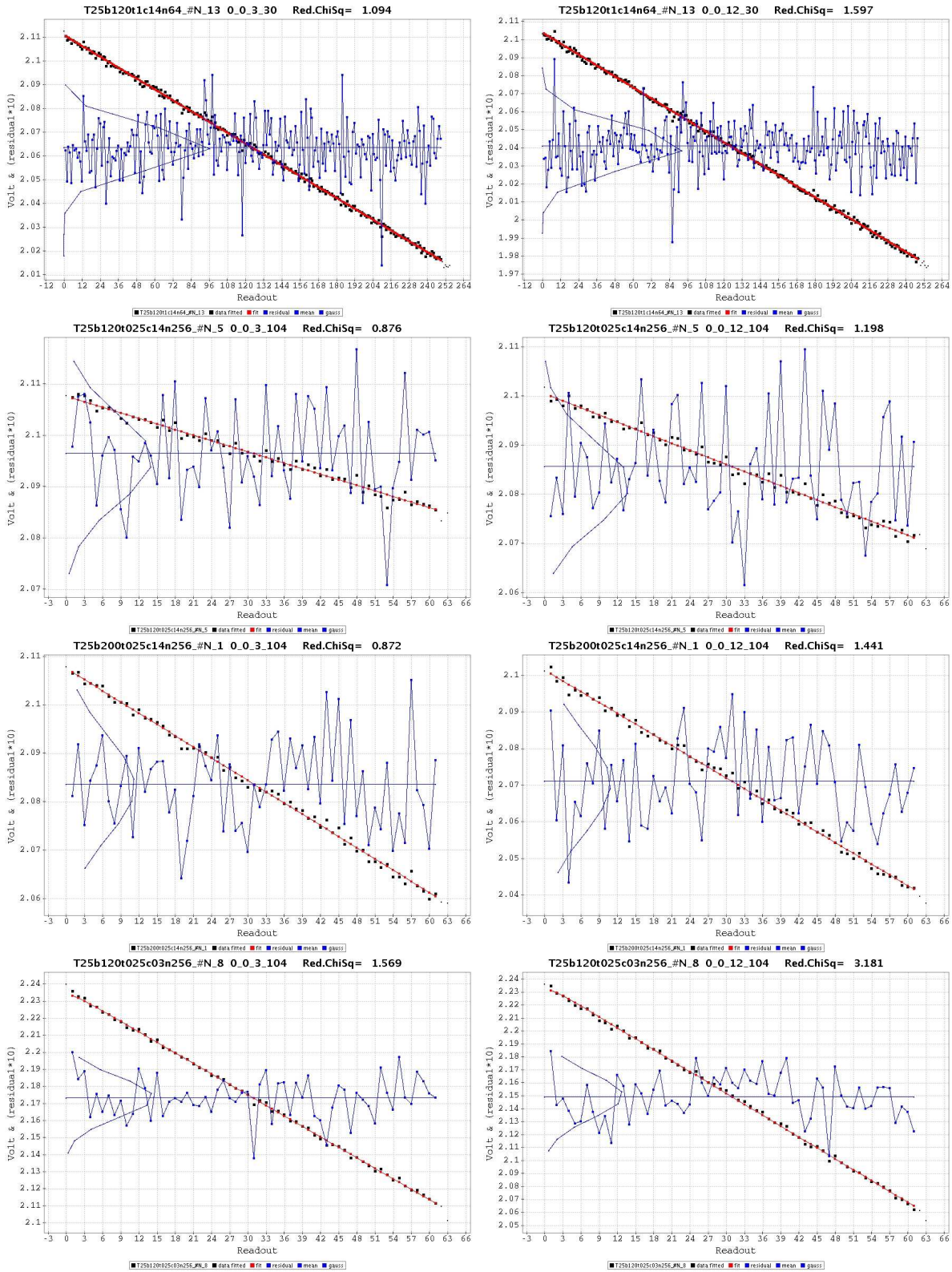


Figure 5: Selected pre-beam fits for different combinations of ramp-length, bias and capacitance. Plotted are Volts versus read-out number. On the left for detector 3, on the right for detector 12. The red points are the fits to the thick black points. Smaller black points are read-outs not considered in the fitting (last read-out, saturation, etc). The blue dots and line represent the residual,  $TEN * (\text{observed} - \text{fitted})$ , shifted to the mean voltage, indicated by the blue horizontal line. The other blue line is a Gaussian fit to a 9-bin histogram of these residuals. At the top of the plots are listed: the file name, the indices  $i_j.k_l$ , indicating the file number in the full list of files analysed, Module, Detector, Ramp, and the reduced Chi-square.

Table 3: Pre-beam data: Summary of fit results with Ramp6Model for detectors 3 (cols. 2-6) and 12 (cols. 7-11).

Name	slope	STDDEV (slope)	calls	$\chi^2_{\text{red}}$	noise ( $10^{-4}$ )	slope	STDDEV (slope)	calls	$\chi^2_{\text{red}}$	noise ( $10^{-4}$ )	(S/N)
N1	-0.20273	0.00236	8	0.97	8.8	-0.25614	0.00232	8	1.53	12.0	1374/1766
N2	-0.46742	0.00392	8	1.21	10.0	-0.59247	0.00477	8	1.95	13.4	1907/1987
N3	-0.83332	0.00475	8	2.71	16.8	-1.06430	0.00602	9	4.09	21.0	2807/2828
N4	-1.32040	0.00769	9	6.48	30.7	-1.69580	0.00980	10	9.89	38.2	2750/2769
N5	-0.09531	0.00190	8	0.95	8.6	-0.12770	0.00230	8	1.56	12.2	802/888
N6	-0.21603	0.00214	8	1.08	9.3	-0.29126	0.00300	8	1.74	13.1	1615/1553
N7	-0.37449	0.00280	8	1.38	10.8	-0.51039	0.00382	8	2.28	14.6	2139/2137
N8	-0.58617	0.00556	8	1.87	12.2	-0.79833	0.00573	9	3.12	16.9	1686/2229
N9	-0.06178	0.00177	7	0.96	8.7	-0.08434	0.00251	8	1.53	11.9	558/537
N10	-0.13822	0.00234	7	1.01	9.3	-0.19052	0.00288	8	1.68	13.0	945/1058
N11	-0.23705	0.00318	8	1.31	10.5	-0.32854	0.00340	8	1.93	13.5	1192/1546
N12	-0.37416	0.00380	8	1.85	12.2	-0.51442	0.00448	8	2.25	14.2	1575/1837
N13	-0.09973	0.00038	8	0.89	8.6	-0.13316	0.00047	10	1.52	12.3	2100/2266
N14	-0.09908	0.00077	9	0.92	8.7	-0.13208	0.00096	9	1.52	12.1	1455/1556
N15	-0.09838	0.00175	7	0.94	8.5	-0.13101	0.00231	8	1.55	12.4	899/907
N16	-0.09852	0.00527	6	1.05	8.9	-0.13034	0.00704	6	1.72	12.6	428/419
N17	-0.10203	0.01544	5	1.80	11.8	-0.13425	0.02183	5	2.88	19.5	150/138
N27	-0.09308	0.00192	7	0.95	8.9	-0.12572	0.00237	8	1.59	12.3	
N28	-0.20940	0.00304	8	1.08	9.2	-0.28652	0.00339	8	1.72	13.2	
N29	-0.36475	0.00373	8	1.40	10.8	-0.50222	0.00505	8	2.24	14.7	
N30	-0.56992	0.00590	9	1.89	12.5	-0.78544	0.00609	9	2.98	16.5	
N31	-0.06025	0.00168	7	0.94	8.5	-0.08259	0.00229	7	1.57	12.3	
N32	-0.13477	0.00231	7	1.07	9.1	-0.18715	0.00271	8	1.69	12.8	
N33	-0.23142	0.00272	8	1.30	10.3	-0.32218	0.00353	8	1.93	13.3	
N34	-0.36528	0.00366	8	1.88	12.7	-0.50507	0.00526	9	2.30	14.1	

#### 4. Low-proton flux data files L65-L78

This section deals primarily with the data taken over a time span of slightly under 1 hour under low proton flux (files T25b120t025c14n1024\_#L\_65.dat to T25b120t025c14n1024\_#L\_78.dat).

Each file consists of 1024 ramps of 0.25 seconds, with a bias value of 120 mV and 1.42 pF capacitance.

All ramps of detectors 3 and 12 have been fitted with the IMEC model with  $R_p$  (i.e. *slope*) as only variable. A simple edge-detection-algorithm was used to detect the strongest glitches. No correction for the glitch was attempted and so only the part of the ramp prior to the glitch is fitted.

Figures 6 and 7 shows selective fits to the ramps. Compared to the tests on the stressed modules the ramps are less well behaved (also see RD 6): there are positive glitches, and some ramps become really “curved”.

Figure 8 shows *slope* for the sequences of files L1-L37, L65-L78, L79-L117.

Table 5 collects these results in quantitative form for files L65-L78. The table also lists the standard deviation over the slopes. One iteration of sigma-clipping is performed where 5 sigma outliers are removed, in order to compute the listed values. It also shows how the (S/N) decreases with increasing radiation.

Table 4: Pre-beam data, *with detector zero subtracted*: Summary of fit results with Ramp6Model for detectors 3 (cols. 2-6) and 12 (cols. 7-11).

filename	slope	STDDEV(slope)	#calls	$\chi^2_{\text{red}}$	noise ( $10^{-4}$ )	slope	STDDEV(slope)	#calls	$\chi^2_{\text{red}}$	noise ( $10^{-4}$ )
N5	-0.09156	0.00225	7	1.32	9.0	-0.12360	0.00264	7	2.67	16.3
N6	-0.20933	0.00241	8	1.45	9.7	-0.28436	0.00312	8	2.89	16.9
N7	-0.36673	0.00315	8	1.81	11.2	-0.50243	0.00414	9	3.43	18.3
N8	-0.57641	0.00514	9	2.07	12.4	-0.78931	0.00593	9	4.30	20.0
N31	-0.05735	0.00211	7	1.55	10.8	-0.080137	0.00270	7	2.05	13.0
N32	-0.12973	0.00279	8	1.60	11.0	-0.181910	0.00307	8	2.17	13.7
N33	-0.22489	0.00304	8	1.74	11.9	-0.315980	0.00371	8	2.27	14.0
N34	-0.35895	0.00378	8	2.20	13.3	-0.499075	0.00538	9	2.62	14.9

Table 5: Summary of fit results with Ramp6Model for detectors 3 (cols. 2-6) and 12 (cols. 7-11) for the series of files T25b120t025c14n1024\_#L\_65 through L\_78.

Name	slope	STDDEV (slope)	calls	$\chi^2_{\text{red}}$	noise ( $10^{-4}$ )	slope	STDDEV (slope)	calls	$\chi^2_{\text{red}}$	noise ( $10^{-4}$ )	(S/N)
L65	-0.096462	0.00190	8	0.965	8.64	-0.12952	0.00241	8	1.548	12.2	1624/1719
L66	-0.096902	0.00198	8	0.975	8.68	-0.13017	0.00247	8	1.527	12.2	1566/1686
L67	-0.104050	0.00464	7	0.977	8.84	-0.13699	0.00476	8	1.551	12.3	717/920
L68	-0.120355	0.00592	7	0.983	8.83	-0.15291	0.00809	8	1.573	12.3	650/604
L69	-0.133070	0.00526	8	0.970	8.81	-0.17295	0.00829	8	1.570	12.3	809/667
L70	-0.152360	0.00628	8	0.978	8.70	-0.19285	0.00562	8	1.575	12.3	776/1098
L71	-0.170100	0.00823	8	0.962	8.68	-0.22258	0.01016	8	1.591	12.2	661/701
L72	-0.207320	0.01250	8	0.994	8.84	-0.24264	0.01136	8	1.589	12.3	530/683
L73	-0.238080	0.00669	8	0.997	8.84	-0.28092	0.01233	8	1.580	12.3	1138/729
L74	-0.271260	0.01493	8	1.009	8.95	-0.30788	0.00892	8	1.614	12.3	581/1104
L75	-0.317880	0.00981	8	1.009	9.02	-0.33152	0.01509	8	1.628	12.4	1036/703
L76	-0.359550	0.01835	8	1.041	9.04	-0.37479	0.00766	8	1.643	12.4	627/1565
L77	-0.414080	0.02643	8	1.003	9.25	-0.40458	0.01130	8	1.656	12.4	501/1145
L78	-0.517590	0.03574	8	0.900	9.32	-0.43800	0.02015	8	1.658	12.4	463/695

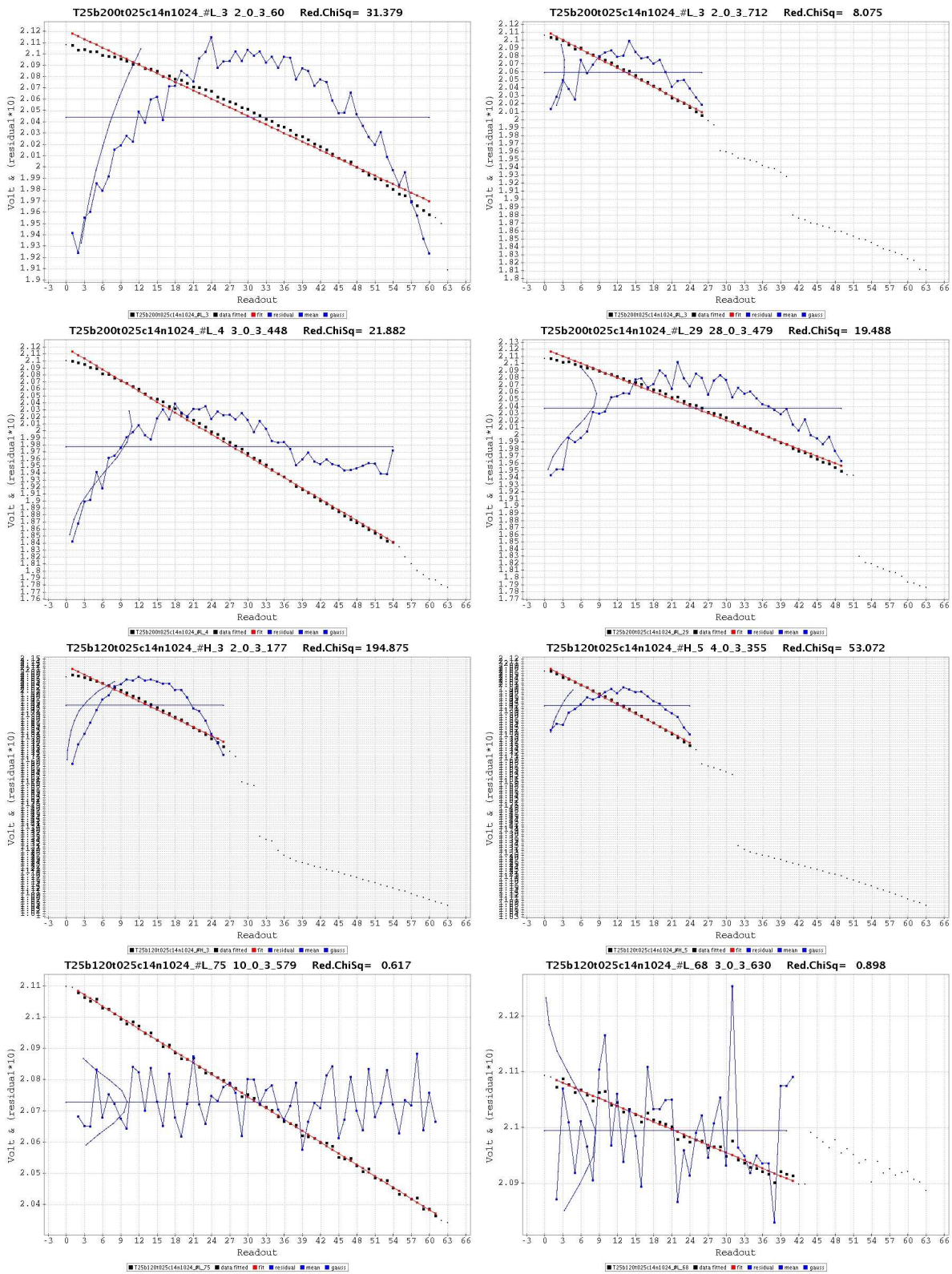


Figure 6: Selective fits for detector 3 of the irradiation data. Both good fits and a-typical behaviour is illustrated. Note the very curved ramps, and a “positive glitch” in the last ramp.

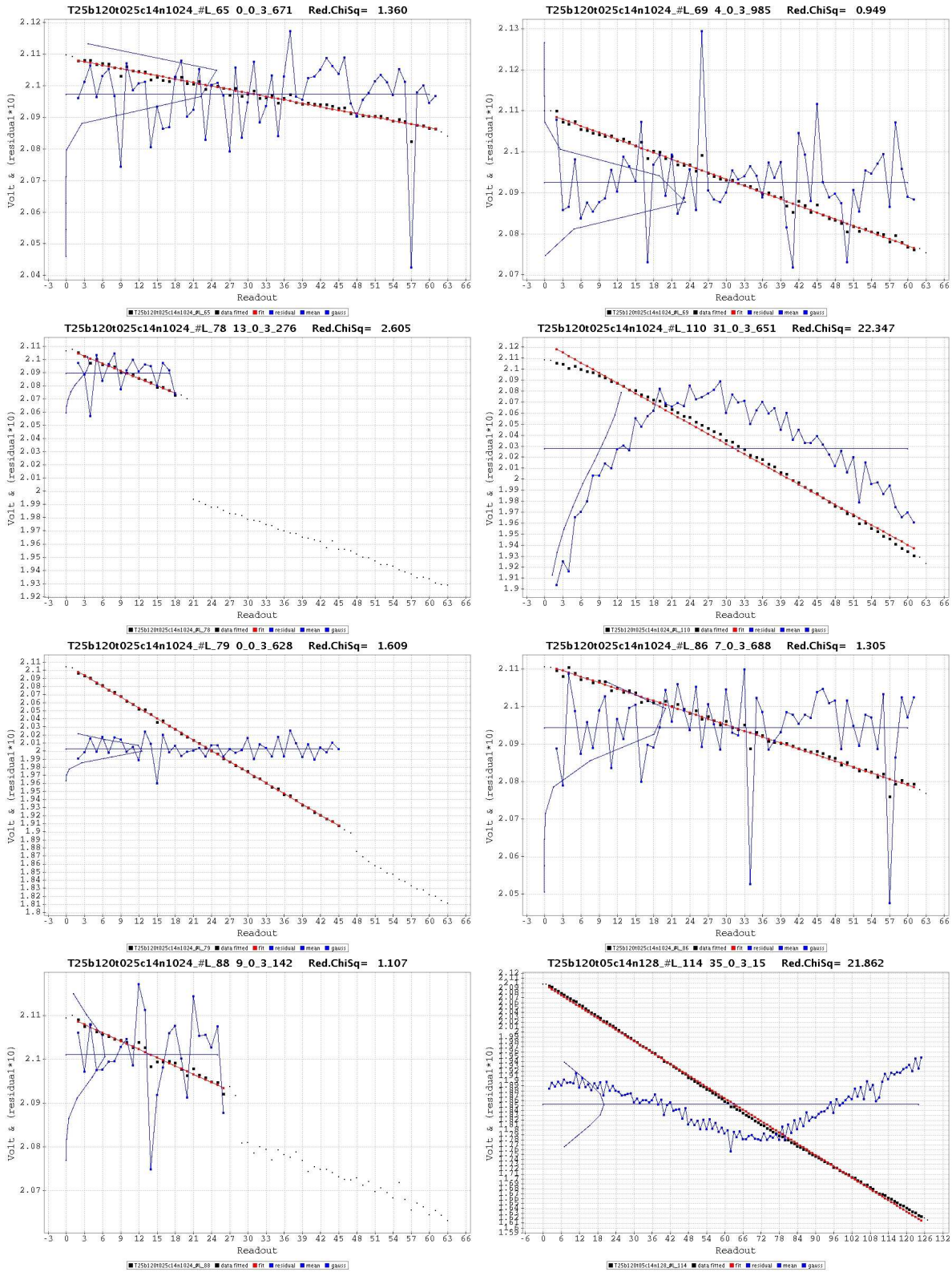


Figure 7: Continued. Selective fits for detector 3 of the irradiation data. Both good fits and a-typical behaviour is illustrated.

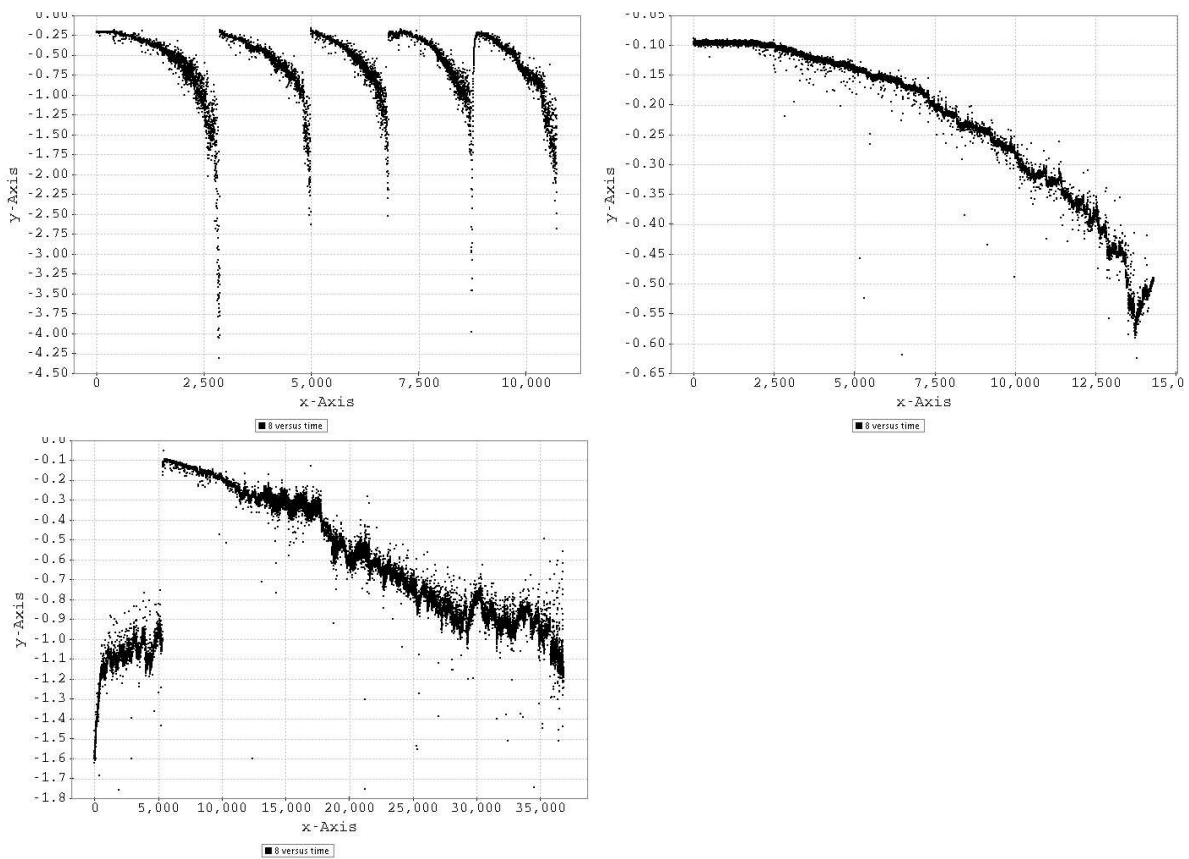


Figure 8: Slope (V/s) versus consecutive ramp number for detector 3 of the time series L1 to L37, L65 to L78, and L79 to L117 (left to right, top to bottom). In the first plot the effect of different curing attempts can be identified. The last plot starts with self-curing after the high proton flux measurements that ended just before, and shows the effect of curing by the flasher.

Table 6: For files L65 - L78: non-destructive readout where the glitch was found.

read-out	number	read-out	number	read-out	number
0	0	22	83	44	62
1	66	23	71	45	82
2	82	24	80	46	77
3	53	25	77	47	60
4	61	26	65	48	57
5	73	27	75	49	78
6	79	28	61	50	77
7	71	29	83	51	78
8	81	30	78	52	80
9	64	31	74	53	76
10	76	32	74	54	68
11	83	33	75	55	74
12	73	34	60	56	80
13	67	35	73	57	72
14	93	36	69	58	79
15	75	37	79	59	83
16	67	38	74	60	79
17	78	39	79	61	62
18	79	40	87	62	75
19	80	41	67	63	298
20	71	42	74		
21	81	43	73	all	4881

## 5. Glitches in the Low-proton flux datafiles L65 - L78

Pierre Royers Q-method with two contrast functions and parameters threshold1 = 0.4, threshold2 = 0.2 (RD 2, RD 4) was used as deglitching algorithm.

Table 6 lists the read-out where a glitch was detected summed over all detectors and files, with the results plotted in Figure 9

It is obvious that the algorithm detects an electronic effect in the last-readout rather than a higher glitch rate.

In Table 7 the number of glitches found in each of the detectors is listed, *not counting those in the last readout*. The true number of glitches should statistically be larger by a factor  $64/62 = 1.03$ , as also glitches in the first readout can not be found by the algorithm.

What is remarkable is that the number is **much** smaller in detectors 5 and 13.

To investigate this further the ramps of file L74 of all detectors were fitted with the IMEC model. The results are listed in the third column of Table 7. Clearly the responsivities of those 2 pixels is very much different from the others.

In order to have statistics that can be compared, Table 8 gives the number of glitches as a function of time (that is, from file L65 to L78), excluding readouts 0 and 63, and including only detectors 1,2,3,4 and 12,14,15,16, which have comparable responsivities.

### Theory

Theoretically one expects that the glitch-height is given by (RD 5, RD 2):

$$\Delta V[\text{Volt}] = 0.1986 \Delta E(\text{MeV}) \frac{R[\text{A/W}]}{c_f[\text{pF}] \eta \lambda[\mu\text{m}] E_g[\text{eV}]} \quad (5)$$

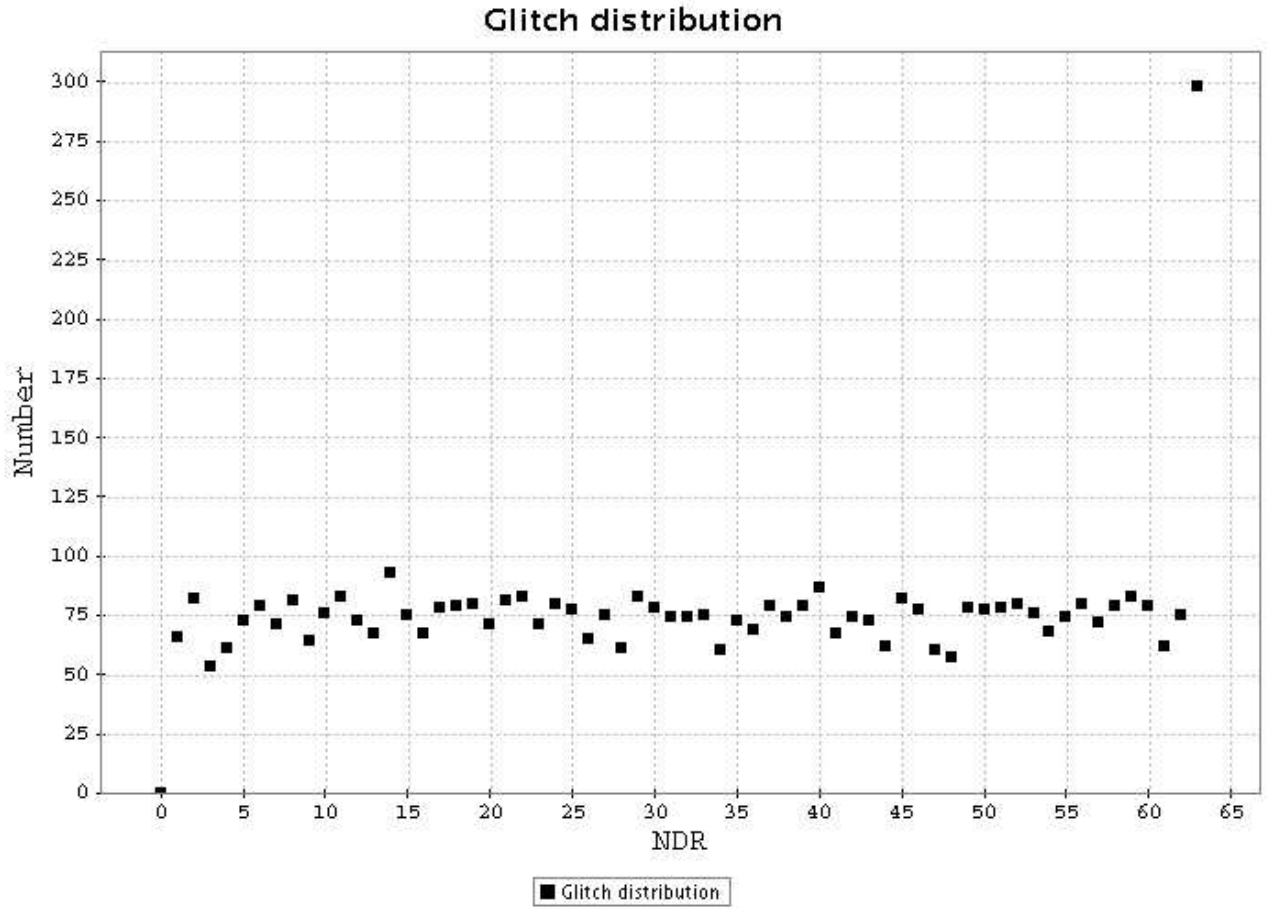


Figure 9: Distribution of glitches found by PR algorithm for files L65-L78 as a function of non-destructive readout number.

with  $R$  the Responsivity,  $E_g$  the energy loss per electron-hole pair produced (2.9 eV for Ge:GA), and  $\eta$  is the quantum efficiency (taken to be 0.3, Poglitsch, private communication).

For the tests with the un-stressed module one can take the wavelength to be  $110 \mu\text{m}$ , and so one may expect the glitches to be of height:

$$\Delta V[\text{Volt}] = 0.00208 \Delta E(\text{MeV}) R[\text{A/W}]/c_f[\text{pF}] \tag{6}$$

depending on the actual responsivity and capacitance used. As the responsivity is defined as:

$$R[\text{A/W}] = c_f \frac{dV}{dt} / P \tag{7}$$

where  $P$  is the infalling power on a pixel ( $[1.3 \text{ and } 1.8] \cdot 10^{-14} \text{ W}$  for detectors 1-8 and 9-16, respectively, according to RD 1). One has therefore as well:

$$\Delta V[\text{Volt}] = 2.08 \Delta E(\text{MeV}) \frac{dV}{dt}[\text{V/s}] / P[10^{-15} \text{ W}] \tag{8}$$

The distribution of energy at the detector surface is listed in Figure 4 of RD 1 and may be approximated by a Gaussian with mean 17.5 MeV and spread 1.5 MeV. An alternative calculation is shown in Figure 3 of RD 1 and may be approximated by a Landau distribution (see RD 5) with mean  $E_p = 9.0 \text{ MeV}$  and width  $R = 3.0$  although this does not reproduce the

Table 7: Distribution of glitches over the detectors for files L65 - L78.

det.	number	median <i>slope</i> in file L74
1	271	$-0.23792 \pm 0.0173$
2	248	$-0.23783 \pm 0.0210$
3	294	$-0.27118 \pm 0.0145$
4	296	$-0.26891 \pm 0.0066$
5	15	$-0.08777 \pm 0.0041$
6	335	$-0.30485 \pm 0.0145$
7	620	$-0.49853 \pm 0.0331$
8	360	$-0.34240 \pm 0.0219$
9	196	$-0.22498 \pm 0.0090$
10	192	$-0.25134 \pm 0.0065$
11	271	$-0.36257 \pm 0.0136$
12	260	$-0.30817 \pm 0.0088$
13	26	$-0.12095 \pm 0.0036$
14	368	$-0.35266 \pm 0.0177$
15	565	$-0.33337 \pm 0.0141$
16	266	$-0.28558 \pm 0.0111$
total	4583	

short tail below 8 MeV. It is shown below (and it was already noted in the analysis of the March 2004 irradiation tests, see RD 5) that this has little to do with the distribution of deposited energy!

To compare theory with observations, the results of PRs algorithm on files L76-L78 are considered (see Table 8).

The black histogram in Figure 10 shows the distribution over glitch height of the 1159 events seen in these 3 files, considering 8 pixels and readouts 1- 62. For this particular setting we know from the results on the simulated data that PR algorithm is about 80% complete with only 2% false detection.

Putting in numbers from Table 5 and the infalling power, we expect  $\Delta V[\text{Volt}] = 0.055 \Delta E(\text{MeV})$ . In a numerical code we simulated  $(1159/0.80)$  events distributed according to a Landau distribution, and made an eye-ball fit to the observations, represented as the red histogram. The parameters for a single Landau distribution are a mean energy of 0.1 MeV, and a “material constant” ( $R$ ) of 10.

What is potentially interesting in the observed distribution is the apparent second peak at 0.032 V. This predicted by RD 7 and suggested to be related to the fact that the cryostat was inclined w.r.t. the beam and the fact that the pixels are located in a non-uniform cavity.

An eye-ball fit with two Landau distributions was also made where  $R$  was used the same. The parameters are the 2 mean energies and the number of events at the higher energies. We find  $R= 11.5$ , mean energies of 0.1 and 0.55 MeV, 200 of the generated 1450 events at the high energy. An alternative interpretation (but not supported by RD 7) is that we see the division between primary and secondary events.

This distribution(s) is (are) very different from the ones calculated for the energy at the detector surface, both in mean energy but also in width: the distribution of energy at the detector surface are rather narrow, while this is clearly inconsistent with the observed glitch height distribution.

The number of events observed in files L76-L78 corresponds to a rate of  $1159 * (64/62 \text{ readouts}) * (16/8 \text{ pixels}) / 768 \text{ sec} / 0.24 \text{ sq.cm} = 13.0 (s^{-1} \text{cm}^{-2})$ . Corrected for the detection efficiency of the detection algorithm a glitch rate rate of  $16.2 (s^{-1} \text{cm}^{-2})$  is derived. If the division between primary and secondary events noted above is correct than the eye-ball fit indicates a glitch rate rate of  $2.2 (s^{-1} \text{cm}^{-2})$  for the primary events and  $14.0 (s^{-1} \text{cm}^{-2})$  for the secondary events.

The beam was set to a nominal value of 10 protons ( $s^{-1} \text{cm}^{-2}$ ). As the observed total rate is larger, this supports the idea that both primary and secondary events are detected.

Table 8: Summary of glitches found (excluding readout 0 and 63). The number is for detectors (1,2,3,4), respectively (12,14,15,16) for the case with and w/o the FIR cut-on filter.

filenames	time (s)	number
L65	256	0/2
L66	256	2/4
L67	256	30/22
L68	256	30/40
L69	256	49/46
L70	256	53/58
L71	256	78/82
L72	256	85/88
L73	256	95/96
L74	256	112/133
L75	256	91/213
L76	256	131/202
L77	256	165/265
L78	256	188/208

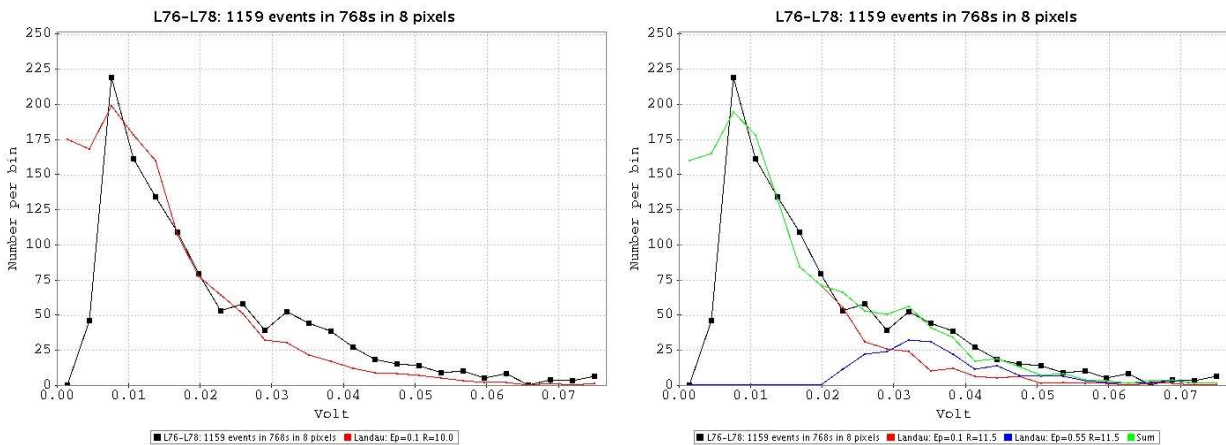


Figure 10: Distribution of glitches found by PR algorithm for files L76-77-78 (black histogram), and eye-ball fit of one (left panel) and two (right panel) Landau distributions of 1.25 times as many events (red and blue histograms).

On the other hand, given the experience over the 3 test campaigns with the calibration of the beam, it can not be excluded that all events are primary events.

## 6. Behaviour at the responsivity plateau; files L113 - L152

Towards the end of day 2 the beam was left sufficiently long on for the responsivity to reach a plateau. Then ramps were recorded at various bias values and ramp lengths at a capacitance of 1.4 pF. The latter is unfortunate as it was shown that intrinsically larger (S/N) can be achieved at lower capacitor values.

As before, the ramps were deglitched and the part before the first glitch fitted with the IMEC model. The median and standard deviation of the *slope* were determined, and 5 sigma outliers removed, to arrive at the final values listed in Table 9

Contrary to the pre-irradiation data, there is no clear tendency for the higher bias values to give higher (S/N). In fact, the tendency is even to the opposite as the best fits to the individual ramps (as judged from the  $\chi^2_{red}$ ) is achieved for bias values  $\lesssim 150$  mV. For the 80 mV bias the  $\chi^2_{red}$ , noise, and (S/N) are only slightly worse than in their pre-irradiation case.

A likely explanation is that the strength of the glitch depends on the slope (Equation 8), and for the low bias the slope

Table 9: Summary of fit results with Ramp6Model for detectors 3 (cols. 2-6) and 12 (cols. 7-11) for the series of files L113 - L152.

Name	slope	STDDEV (slope)	calls	$\chi^2_{red}$	noise ( $10^{-4}$ )	slope	STDDEV (slope)	calls	$\chi^2_{red}$	noise ( $10^{-4}$ )	(S/N)
T25b200t1c14n64_#L_148	-1.9187	0.1255	9	5.9	25.0	-1.6529	0.09226	8	15.1	28.8	68/62
T25b200t05c14n128_#L_149	-1.7172	0.1005	10	33.2	75.8	-1.5016	0.04988	10	30.6	68.8	146/312
T25b200t025c14n256_#L_150	-1.7313	0.0458	9	4.6	20.8	-1.5520	0.06027	9	5.0	21.3	592/403
T25b200t0125c14n512_#L_151	-1.7661	0.0888	9	2.0	13.3	-1.8278	0.16774	9	7.7	33.0	434/221
T25b200t00625c14n1024_#L_152	-1.9033	0.1432	9	2.3	15.5	-1.7946	0.25135	9	5.2	30.1	404/198
T25b180t1c14n64_#L_138	-1.5759	0.0826	9	3.6	38.7	-1.4128	0.08249	11	42.0	67.4	79/84
T25b180t05c14n128_#L_139	-1.3968	0.0352	10	24.0	75.3	-1.4755	0.12051	9	21.6	56.2	436/127
T25b180t025c14n256_#L_140	-1.4431	0.0298	9	2.1	14.1	-1.5291	0.04934	9	3.8	20.3	768/483
T25b180t0125c14n512_#L_141	-1.4999	0.0708	9	1.6	11.5	-1.5631	0.08135	9	3.0	17.9	470/424
T25b180t00625c14n1024_#L_142	-1.5987	0.1300	9	2.1	14.5	-1.4579	0.08590	8	3.3	17.9	382/532
T25b160t1c14n64_#L_133	-1.2601	0.0635	11	34.5	65.9	-1.3454	0.10550	11	35.9	68.1	133/70
T25b160t05c14n128_#L_134	-1.2382	0.0315	9	16.2	58.3	-1.3479	0.04328	10	21.8	62.0	433/338
T25b160t025c14n256_#L_135	-1.4548	0.0574	9	3.3	16.8	-1.3470	0.03634	9	2.3	14.7	393/588
T25b160t0125c14n512_#L_136	-1.4302	0.0456	9	1.4	10.6	-1.2475	0.03048	9	1.9	13.3	703/922
T25b160t00625c14n1024_#L_137	-1.3661	0.0681	8	1.9	12.1	-1.3267	0.09480	8	3.3	17.7	633/440
T25b140t025c14n256_#L_130	-1.2388	0.0543	9	1.3	10.8	-1.0665	0.02807	9	1.9	13.3	362/606
T25b140t0125c14n512_#L_131	-1.3163	0.0662	9	1.4	10.5	-1.1320	0.06859	9	2.1	14.1	445/370
T25b120t025c14n256_#L_115	-0.9916	0.0409	9	1.3	10.2	-0.7875	0.02898	8	1.7	12.7	386/435
T25b120t0125c14n512_#L_116	-0.9505	0.0280	8	1.3	10.2	-0.8110	0.01861	8	1.9	13.2	764/984
T25b80t1c14n64_#L_123	-0.5748	0.0116	10	10.7	42.4	-0.5531	0.00706	11	7.6	31.8	395/626
T25b80t05c14n128_#L_124	-0.5695	0.0086	9	1.1	10.0	-0.5842	0.00919	9	1.7	12.2	742/720
T25b80t025c14n256_#L_125	-0.5587	0.0155	8	1.1	9.6	-0.5875	0.01160	8	1.7	12.6	572/808
T25b80t0125c14n512_#L_126	-0.5913	0.0148	8	1.2	9.5	-0.5764	0.01815	8	1.9	12.7	901/715
T25b80t00625c14n1024_#L_127	-0.5558	0.0220	7	1.9	12.4	-0.5880	0.02701	7	3.0	17.4	798/688

is the most shallow one. That is, the glitch will increase the noise but will have a less devastating effect on the overall behaviour of the ramp.

A second conclusion is that the best (S/N) are achieved for a ramp-lengths of 1/4 and 1/8 seconds.

Table 10 lists the integrating noise, with the post-integration noise fixed at 100 E(-5), respectively, 128 E(-5) for detector 3 and 12 for a capacitance of 1.4 pF (see Table 1).

Next to the filename, between brackets, is the corresponding filename from Table 1. The integrating noise is increased by factors of 20 or more. This direct comparison is not correct however, as in the pre-irradiation data the integration noise depends on the slope. In the last column is the integration noise listed expected for that slope. The irradiation results in an effective increase in the integration noise by a factor of 3.

Table 10: Integration noise.

filename	detector	integration noise ( $10^{-6}$ )	expected integration noise
T25b200t025c14n256.#L_150 (N1)	3	$1229 \pm 8$	404
	12	$1485 \pm 20$	374
T25b120t025c14n256.#L_115 (N5)	3	$1450 \pm 19$	273
	12	$850 \pm 12$	232
T25b80t025c14n256.#L_125 (N9)	3	$500 \pm 7$	183
	12	$369 \pm 7$	190

## 7. Conclusions

The pre-irradiation tests suggests that the highest (S/N) is reached for the highest bias (200 mV), longest integration time (1s), and a low capacitance of 0.3 or 0.4 pF.

The irradiation data suggests, for a fixed capacitance, a low bias value (perhaps in the range 80-140 mV) and a ramp length of 1/4 or 1/8s.

The Q-test based glitch detection algorithm results in a glitch rate of  $16 (s^{-1}cm^{-2})$  compared to the nominal value of  $10 (s^{-1}cm^{-2})$ .

As found before for the two earlier test campaigns the observed glitch distribution can be translated to a mean energy deposited in the detector which is significantly lower than the mean energy at the crystal surface. For the present campaign the mean energy deposited is 0.1 MeV, while the energy at the crystal surface is 10 MeV.